Experimental study of unsteadiness in supersonic shock-wave/turbulent boundary-layer interactions with separation

D. Estruch, D. G. MacManus, D. P. Richardson, N. J. Lawson, K. P. Garry and J. L. Stollery
Department of Aerospace Sciences
Cranfield University
Cranfield, UK

ABSTRACT

Shock-wave/turbulent boundary-layer interactions (SWTBLIs) with separation are known to be inherently unsteady but their physical mechanisms are still not totally understood. An experimental investigation has been performed in a supersonic wind tunnel at a freestream flow Mach number of 2·42. The interaction between a shock wave created by a shock generator (α = 3º, α = 9º, α = 13º and α = 15º deflection angles) and a turbulent boundary layer with thickness δ = 5mm has been studied. High-speed Schlieren visualisations have been obtained and used to measure shock wave unsteadiness by means of digital image processing. In the interactions with separation, the reflected shock's unsteadiness has been in the order of 10^2Hz. High-speed wall pressure measurements have also been obtained with fast-response micro-transducers along the interactions. Most of the energy of the incoming turbulent boundary layer is broadband and at high frequencies (>10^4Hz). An addition of low-frequency (<10^4Hz) fluctuation energy is found at separation. Along the interaction region, the shock impingement results in an amplification of fluctuation energy due to the increase in pressure. Under the main recirculation region core there is only an increase in high frequency energy (>10^4Hz). Amplification of lower frequency fluctuation energy (>10^3Hz) is also observed close to the separation and reattachment regions.

NOMENCLATURE

f	frequency, Hz
$G(f)$	power spectral density of pressure signal, $= \lim_{\Delta f \to 0} \frac{1}{(\Delta f)} \left(\lim_{t_f \to \infty} \frac{1}{t_f} \int_0^{t_f} p^2(t, f, \Delta f)\, \mathrm{d}t \right)$
$H(f)$	power spectral density of shock displacement in streamwise direction, $= \lim_{\Delta f \to 0} \frac{1}{(\Delta f)} \left(\lim_{t_f \to \infty} \frac{1}{t_f} \int_0^{t_f} x_s^2(t, f, \Delta f)\, \mathrm{d}t \right)$
kurtosis	kurtosis coefficient, $= \frac{\frac{1}{n}\sum_{i=1}^{n}\left(p_i - \overline{p}\right)^4}{\sigma_p^{\,4}}$
K	pressure transducer (K1 to K5)
L	interaction length, m
M	Mach number
n	number of data points
p	wall static pressure, Pa

Paper No. 3466. Manuscript received 10 June 2009, accepted 29 January 2010.

https://doi.org/10.1017/S0001924000003742 Published online by Cambridge University Press

$p(t,f,\Delta f)$ $p(t)$ in the frequency range from f to Δf
p wall static pressure fluctuation, Pa
$\overline{p}$ arithmetic mean of pressure signal, $= \frac{1}{n}\sum_{i=1}^{n} p_i$
P probability distribution of pressure signal, where $\sum_{i=1}^{n} P_i = 1$
r recovery factor for a turbulent boundary layer, assumed $r = 0{\cdot}9$.
Re/m Reynolds number per unit length, $= \frac{\rho U}{\mu}$
Skewness skewness coefficient = $\frac{\frac{1}{n}\sum_{i=1}^{n}\left(p_i - \overline{p}\right)^3}{\sigma_p^{\,3}}$
S boundary-layer separation locus
St Strouhal number, $= fl/U_\infty$
t time, s
T static temperature, K
U velocity in streamwise direction, ms^{-1}
x distance in streamwise direction, m
x_s shock displacement in streamwise direction, m
$\overline{x_s}$ mean location of shock in streamwise direction, m
$x_s(t, f, \Delta f)$ $x_s(t)$ in the frequency range from f to Δf
y distance from top wall in vertical direction, m
α shock generator deflection angle, °
δ boundary layer thickness with edge at $U = 0{\cdot}99U_\infty$, m
θ shock angle, °
μ dynamic viscosity, Pa·s
ρ density, kg·m^{-3}
σ_p standard deviation of pressure signal, $= \left(\frac{1}{n-1}\sum_{i=1}^{n}\left(p_i - \overline{p}\right)^2\right)^{1/2}$

Subscripts

1 conditions upstream of shock
2 conditions downstream of shock
∞ freestream conditions
aw adiabatic wall
e conditions at boundary-layer edge
f final
i instantaneous
min minimum value
o total conditions or conditions just upstream of interaction
w conditions on wall

1.0 INTRODUCTION

Shock-wave/turbulent boundary-layer interactions (SWTBLIs) are of high importance in aerospace engineering[1-6]. For instance, a shock wave impinging on the boundary layer on the surface of a high-speed vehicle may affect its performance due to the local increase in static pressure and aerodynamic heating[7]. The same effects may also be found in internal aerodynamics, e.g. engine intakes, rotors, etc[8]. Supercritical interactions occur when the adverse pressure gradient imposed by the incident shock wave is strong enough so as to cause local separation of the boundary layer. In these interactions, a reflected shock is found upstream of the separation bubble followed by an expansion region and a reattachment shock as the boundary layer reattaches to the wall. These interactions are known to be inherently unsteady and result in fluctuating loads that need to be predicted in many aerospace applications[9,10]. Whereas high frequencies (≈10^{4}Hz) are attributed to the turbulent nature of the flow[11], the low frequency unsteadiness that characterises the oscillation of the reflected shock is not totally understood as yet[12,13]. Two different potential sources have been considered to date: the incoming boundary layer and the downstream separation bubble[14].

Seminal quantitative studies on the unsteadiness of separated turbulent boundary layers at supersonic speeds were presented by Kistler[15]. In his work, he obtained fluctuating wall pressure measurements ahead of a forward facing step and observed an increase in power spectra at low frequencies close to the separation region which he linked to the low-speed oscillation of the separation shock seen in high-speed shadowgraph and Schlieren visualisations[16]. Later studies suggested that the separated shear layer could result in a low frequency motion of the subsonic bubble which would consequently provoke the oscillation of the separation shock[17]. This hypothesis was also backed in later experimental work that linked the low frequency motion of the reflected shock with the expansion and contraction of the separation bubble[18,19].

Contrarily, other investigations suggested that such low-frequency unsteadiness could be principally due to fluctuations in the incoming boundary layer. Plotkin[20] proposed a simple model where velocity fluctuations in the boundary layer resulted in a change in the shock's location. A direct correlation between pressure fluctuations in the incoming boundary layer and the separation shock was later reported by Erengil and Dolling[18] and more advanced measurements found a direct relationship between positive streamwise velocity fluctuations in the incoming boundary layer and the motion of the separation shock's foot using particle image velocimetry (PIV) and high-speed wall pressure measurements[21]. Although no correlation was found between variations in the incoming boundary layer thickness and the motion of the foot of the separation shock, the latter was noticed to be farther downstream when the boundary layer mean velocity profile was momentarily fuller due to its increased resistance to separation. Correlation between the motion of the separation shock and the thickening/thinning of the incoming boundary layer was later shown by Bueno *et al*[22] based on cinematographic planar laser scattering (PLS) visualisations. In addition, the existence of Göertler vortices in the incoming boundary layer was also proposed as a possible source of low frequency unsteadiness in Ref. 23. More recent investigations by Ganapathisubramani *et al*[24] have also noticed the existence of very-long-coherent structures in turbulent boundary layers (about 50δ-long) whose passage through the shock could trigger such low-frequency unsteadiness.

The present investigation provides new detailed data on the unsteadiness of SWTBLIs with separation. A new method based on high-speed Schlieren visualisations and digital image processing is used to measure the unsteadiness of the reflected shock and high bandwidth wall pressure measurements are used to determine the dominating frequencies and other statistical properties of the flow at different locations along the interactions.

2.0 EXPERIMENTAL SETUP AND MEASUREMENT TECHNIQUES

An experimental investigation has been performed in the Cranfield University 2·5in × 2·5in supersonic suck-down wind tunnel. In this wind tunnel, atmospheric air is drawn through an alumina drying bed before reaching a nozzle liner which determines the Mach number in a working section of 2·5in × 2·5in (63·5mm × 63·5mm). Air is then dumped into a vacuum tank at the other side of the tunnel. The operating freestream Mach number was calculated based on the total pressure measured at the settling chamber of the tunnel and on the static pressure just downstream of the interaction measured by Druck PDCR22 15psi (≈100kPa) differential transducers. The nominal freestream Mach number of 2·42 was estimated to be within ±0·03.

The thickness of the incoming boundary layer just upstream of the interaction was obtained from pitot-probe traverse measurements and estimated to be δ_0 = 5mm (Table 1). The freestream Reynolds number based on boundary-layer thickness was $Re_{\delta_0} = 2{\cdot}6 \times 10^4$, with a stagnation pressure (P_0) in the settling chamber of approximately 99,740 ±285Pa and atmospheric temperature (T_0) of 295K ±3K. The typical total run time was about 20 seconds.

https://doi.org/10.1017/S0001924000003742 Published online by Cambridge University Press

Table 1
Test conditions

M_∞	P_0(kPa)	T_0(K)	δ_0(mm)	Re_{δ_0}
2·42	99·7	295	5	$2{\cdot}6\times10^4$

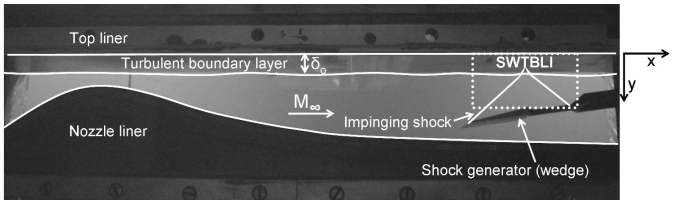


Figure 1. Test arrangement.

Table 2
Shock generator configurations used and corresponding shock angles and theoretical pressure ratios across the incident shock

Shock generator angle (α)	3°	9°	13°	15°
Incident shock angle (θ)	27°	32°	36°	38°
Pressure ratio (p_2, p_1)	1·2	1·7	2·2	2·4

2.1 Experimental setup

SWTBLIs can occur in variety of ways. A basic interaction, commonly investigated, is that which results from an oblique shock wave impinging on a wall boundary layer[6,25]. This interaction has been reproduced in the present study with the shock wave created by a shock generator and impinging onto the fully turbulent boundary layer on the working section top wall (Fig. 1). The shock generator was a two-dimensional wedge with a width of 40mm and placed at the centre of the test section. Different strengths and impinging angles of the shock wave have been obtained by using the shock generator at deflection angles of $\alpha = 3^o$, $\alpha = 9^o$, $\alpha = 13^o$ and $\alpha = 15^o$ with respect to the freestream flow. Larger deflection angles could not be reproduced due to blockage of the test section. The resulting shock angles (θ) and pressure ratios (p_2, p_1) through the shocks used in the present investigation are listed in Table 2.

A subcritical SWTBLI was observed with the shock generator at a deflection angle of $\alpha = 3^o$ and incipient separation was obtained with the shock generator at $\alpha = 9^o$, for which the interaction was identified as critical. Two supercritical SWTBLIs were obtained with the shock generator at $\alpha = 13^o$ and $\alpha = 15^o$. The velocity profile of the incoming boundary layer was determined from pitot-probe traverse measurements and shown to conform to a power law velocity profile $U/U_e = (y/\delta_0)^n$ with an exponent of $n = 5$ (Fig. 2). The total uncertainty of the boundary layer traverse positioning was ±0·11mm.

2.2 High-speed Schlieren visualisations and image processing

The Schlieren technique is a common optical diagnostic used in supersonic and hypersonic wind tunnel testing to image the flow under study[26,27]. High-speed Schlieren is an advanced variance of this technique which acquires time-resolved visualisations that provide information on the flow unsteadiness[28]. The current application uses a digital high-speed Schlieren system developed by Estruch *et al*[29]. In this case, to analyse shock unsteadiness, the location of the shock in each Schlieren image has been determined and the dominant frequencies in the shock motion estimated by means of spectral analysis using a Fourier transform based MATLAB toolbox. An example of a Schlieren image corresponding to a subcritical interaction is shown in Fig. 3 together with the respective binary image which indicates the location of the incident and reflected shocks in the flow. Sets of 2,048 time-correlated images were obtained. At a 10kHz acquisition frame rate the effective bandwidth in this case is 5kHz.

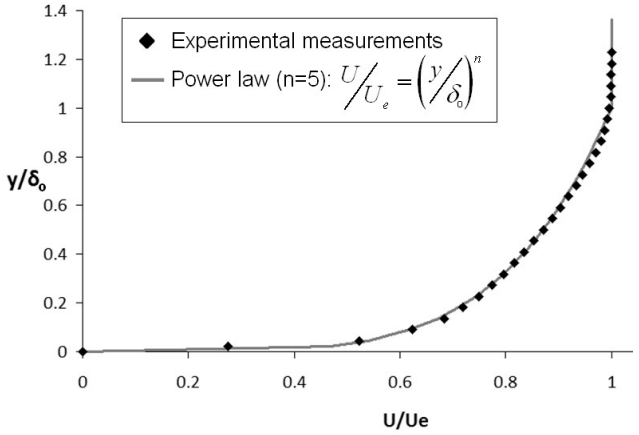
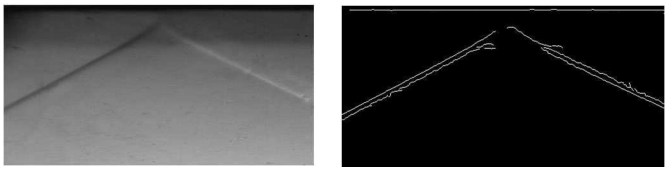


Figure 2. Incoming boundary layer profile.



(a) (b)

Figure 3. Schlieren image of subcritical interaction $\alpha = 3°$ (a) and corresponding binary image indicating the location of the incident and reflected shocks (b). Flow from left to right.

2.3 High-speed wall pressure measurements

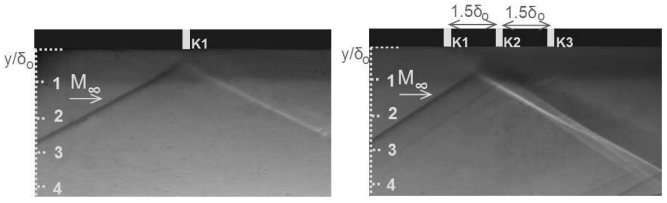
Wall pressure measurements were taken with fast-response pressure transducers (Kulite XCS-062) which were positioned at five locations along the interaction length. Their locations extend from the upstream flow to the relaxation region farther downstream in the interaction (Figs 4 and 5). The transducers have a diameter of 1·7mm and were flush mounted with the surface. They have a range of 0-100kPa and a natural frequency of approximately 200kHz. The transducer output was amplified using a Fylde M14DS (gain = 20) and low-pass filtered using a Fylde 301SF at 50kHz. For each transducer 262,144 samples were acquired using a 16-bit National Instruments BNC-2110 DAQ with a sampling frequency of 100kHz. Ensemble average spectral data was determined by performing FFT analyses on 63 blocks of 8,192 samples with a 50% overlap. Each block was windowed using a Hanning function and a power correction factor of 8/3 was applied to counteract the windowing. The frequency resolution was 12·2Hz.

The typical transducer combined linearity, hysteresis and repeatability error quoted by the manufacturer is ±0·25% full-scale output. The transducers were statically calibrated across their full range (0-100kPa) and the static calibration standard was estimated to have an uncertainty of ±0·13%. Repeatability tests were performed for each configuration. Based on the bias errors and on a statistical analysis of the measurements, an error of ±0·28% is estimated (i.e. ±285Pa relative to atmospheric pressure).

The power spectra of the obtained signals are broadband in nature and contain no dominant frequency. Using the method used by Dupont *et al*[25] and Dussauge *et al*[6], an improved interpretation of the results is obtained by calculating $f{\cdot}G(f)$ in a logarithmic scale where $G(f)$ is the power spectral density of the temporal frequency such that if p is the wall pressure fluctuation:

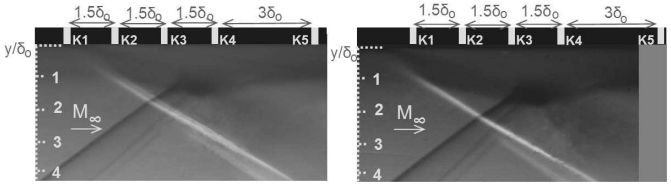
$$\overline{p'^2} = \int_0^\infty G(f)\mathrm{d}f = \int_0^\infty fG(f)\mathrm{d}(\ln f) \quad \ldots (1)$$

https://doi.org/10.1017/S0001924000003742 Published online by Cambridge University Press



(a) (b)

Figure 4. Subcritical SWTBLI α =3° (a) and critical SWTBLI α = 9° (b).



(a) (b)

Figure 5. Supercritical SWTBLI α =13° (a) and α =15° (b).

3.0 ANALYSIS OF RESULTS AND DISCUSSION

The unsteady behaviour of the interactions under study has been investigated based on the high-speed Schlieren and high-bandwidth wall pressure measurements.

3.1 High-speed Schlieren visualisations

The two main factors that determine the strength of the SWTBLI are the upstream nature of the boundary layer and the pressure ratio imposed by the incident shock. SWTBLIs are generally distinguished between those where the boundary layer remains attached to the wall (subcritical) and those where the incident shock is strong enough to cause a boundary layer separation (supercritical). In subcritical interactions, a gradual bending of the impinging shock can be observed as it submerges into the boundary layer and as it is reflected from the embedded sonic line. In supercritical interactions, the separation, and subsequent reattachment, of the boundary layer gives rise to a subsonic bubble, and the reflected shock foot is upstream of the incident shock impingement locus. Critical interactions are those where incipient separation of the boundary layer is present.

The Schlieren visualisations reveal a subcritical interaction for the α = 3° deflection case, a critical interaction at α = 9° deflection and two supercritical interactions at α = 13° and α = 15°. Schlieren snapshot images of these interactions are shown in Figs 4 and 5, indicating the position of the pressure transducers on the wall (K1 – K5).

3.2 Shock unsteadiness

The unsteadiness of the supercritical interactions is qualitatively shown by the high-speed Schlieren videos. It is observed that the incident shock wave remains practically steady for all cases. The reflected shock wave is also essentially steady for the configurations α = 3° and α = 9°. In contrast, the reflected shock is unsteady for the two supercritical interactions (α = 13°, α = 15°). By using the high-speed Schlieren images and applying the method presented in Ref. 28, the change in location of the reflected shock has been quantified (Fig. 6). The amplitude of the reflected shock's displacement at a distance of y/δ_0= 1·5 is approximately 4mm for the α = 13° and α = 15° interactions.

Supercritical interactions reproduced in similar wind tunnel facilities have been reported to be strongly three-dimensional and thus to induce the appearance of 'tornado' vortices on the working section sidewalls which may interfere with the interaction under study[30]. Surface oil visualisations were used to assess the three-dimensionality of the supercritical interactions reproduced in this case and revealed a strongly 3D interaction with a qualitatively similar aspect to that reported by Dussauge *et al*[6], i.e. with a generally longer separation length along the symmetry plane of the tunnel. Considering that Schlieren is a spatially integrating technique and that it is the sharper and most upstream pixel intensity gradients in the image which are identified by the image processing algorithms – and thus used to determine the shock locations – it is the location of the incident and reflected shocks in the tunnel centreline which is considered. Further details on the measurement method can be found in Ref. 29.

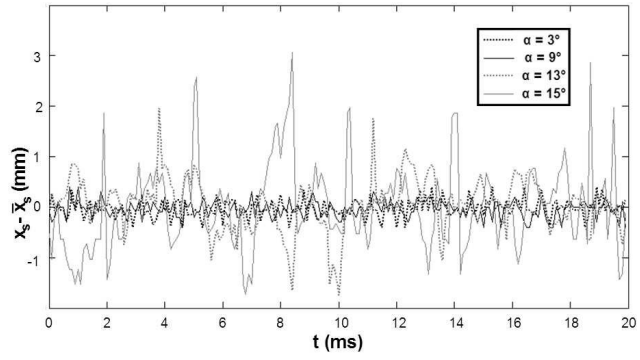


Figure 6. Displacement of reflected shock in streamwise direction with respect to its mean position ($x_s - \bar{x}_s$) as a function of time, at y/δ_0 = 1·5 for the four SWTBLI cases investigated.

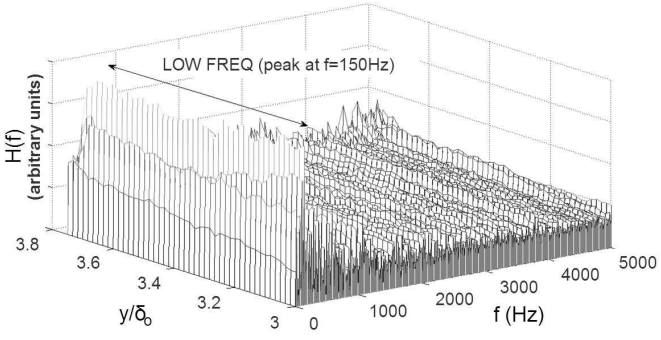
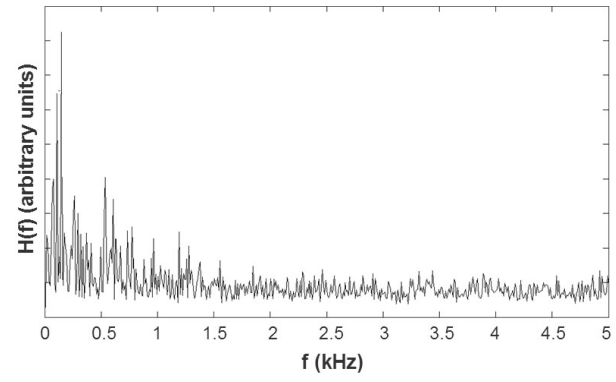


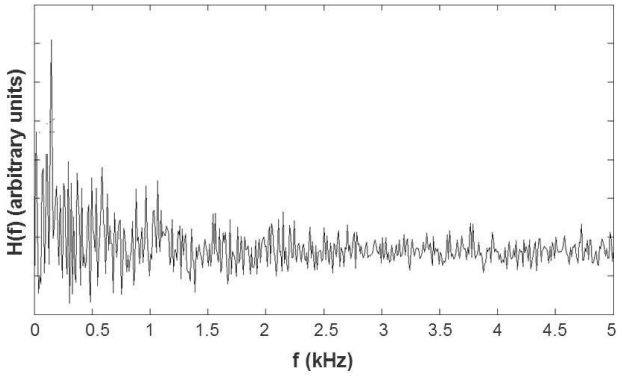
Figure 7. Frequency spectra corresponding to α = 13° SWTBLI along y/δ_0 = 3 to y/δ_0 = 3·75 showing low frequency domination.

A measure of the dominant frequencies in the reflected shock unsteadiness is determined for the two supercritical cases. The spectra of the time-dependent shock locations, $H(f)$, have been calculated along two different regions in the image: upstream of the intersection between incident and reflected shocks (y/δ_0= 1 to y/δ_0= 1·75) and downstream of it (y/δ_0= 3 to y/δ_0= 3·75). A sample carpet plot is shown in Fig. 7 for the α =13° case along y/δ_0= 3 to y/δ_0= 3·75. Results obtained have been averaged through these two regions (y/δ_0= 1 to y/δ_0= 1·75 and y/δ_0= 3 to y/δ_0= 3·75) and are presented in Fig. 8 for the α =13° case and in Fig. 9 for the α = 15° case. No clear periodic motion of the shock is present in any of the cases and the shock unsteadiness is broadband in nature with dominating frequencies of the order of 10^2Hz. Whereas the dominant frequencies in the α = 13° interaction appear to be more concentrated around frequencies of 150Hz, in the α = 15° interaction these are found at slightly higher frequencies (250Hz and 500Hz). In an attempt to non-dimensionalise the shock frequency in terms of Strouhal number ($St = fL/U_\infty$ as defined in Ref. 6) and considering the length of the interaction $L \approx$ 40mm, these measurements correspond to values

https://doi.org/10.1017/S0001924000003742 Published online by Cambridge University Press

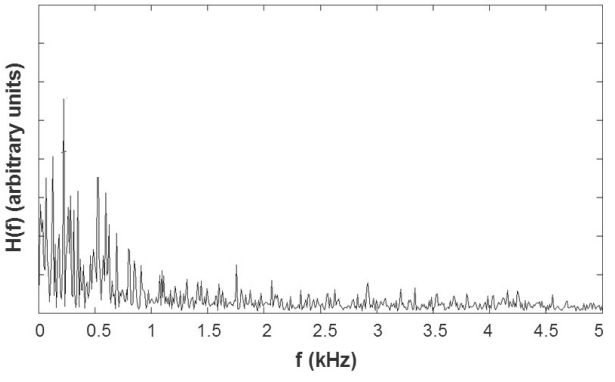


(a)

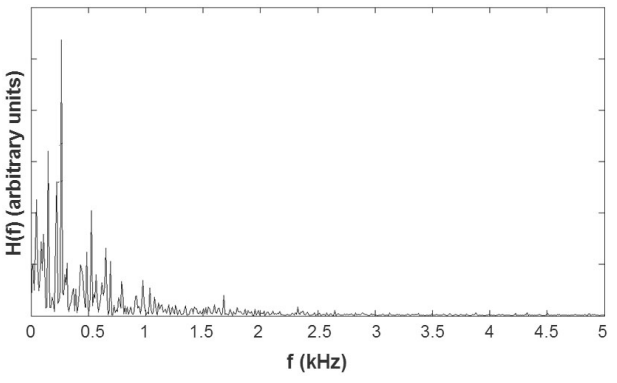


(b)

Figure 8. Frequency spectra corresponding to α = 13° SWTBLI, averaged through y/δ_0 = 1 to y/δ_0 = 1·75 (a) and through y/δ_0 = 3 to y/δ_0 = 3·75 (b).



(a)



(b)

Figure 9. Frequency spectra corresponding to α = 15° SWTBLI, averaged through y/δ_0 = 1 to y/δ_0 = 1·75 (a) and through y/δ_0 = 3 to y/δ_0 = 3·75 (b).

between 0·01 and 0·04. It must be noted, however, that this factor derives from low-speed flow studies[31] and its application to supersonic flows is not established. While it is not clear that a unique value independent of flow conditions should be found, the values obtained in this case are close to the generic value of St = 0·03 mentioned in Ref. 6.

The dominant frequencies of the reflected shock motion are therefore higher for stronger adverse pressure gradients imposed on the boundary layer in this case. Whereas in the α = 13° interaction, frequencies of 150Hz dominate the unsteadiness of the reflected shock both ahead and downstream of its intersection with the incident shock, the incident shock in the α = 15° interaction seems to act as a low-pass filter on the reflected shock's unsteadiness, slightly attenuating the higher frequencies measured ahead of the shock-shock intersection.

3.3 High-speed wall pressure measurements

Different statistical properties of the unsteady pressure measurements obtained are summarised in Table 3. Due to the small extent of the α = 3° interaction, relevant measurements were only taken under the shock impingement location (K1). Three measurement points (K1 – K3) were considered for the α = 9° interaction and 5 points (K1 – K5) along the supercritical ones (α = 13° and α = 15°) due to their longer extent.

About 80% of the energy in the undisturbed boundary layer is at frequencies higher than 10^4Hz. The average wall pressure under the undisturbed boundary layer just ahead of the interactions was $p_{\overline{wo}}$ = 6,630Pa with practically zero skewness and a kurtosis factor of 3, indicating respectively that the data is symmetrical (skewness = 0) and conforms to a Gaussian distribution (kurtosis = 3). The same trend was also observed by Dolling and Or[32] and is characteristic of supersonic turbulent boundary layers[33]. The standard deviation of the incoming boundary layer was σ_{po} = 50Pa, which is significantly lower than the value predicted by the semi-empirical expression of Laganelli *et al*[34] for σ_p in attached supersonic and hypersonic boundary layers as shown in Equation (2). By assuming $T_w = T_0$ and a recovery factor of r = 0·9, σ_p = 114Pa would be expected at the present conditions. This expression has been shown to overpredict σ_p by factors of about 1·3 in previous studies[32] but the significantly greater overprediction in the present case (2·3 greater) indicates that the turbulence level of the incoming boundary layer is likely to be lower than the average turbulent supersonic boundary layer simulated in experimental facilities. This boundary layer is thus thought to be more prone to separation. This is consistent with the fact that incipient separation of the boundary layer occurred using a shock generator deflection angle of 9° while according to Kuehn[35], who used a similar test rig to study incident SWTBLIs, incipient separation of a supersonic turbulent boundary layer at these conditions would occur using a 10°-deflected shock generator.

$$\sigma_p = \frac{0{\cdot}0042 M_e^2 p_e}{\left[1 + 0{\cdot}13 M_e^2\right]^{0{\cdot}64}} \quad \ldots (2)$$

The impingement of the shock wave on the boundary layer results in an increase in static pressure along the interaction. In the super-

https://doi.org/10.1017/S0001924000003742 Published online by Cambridge University Press

Table 3
Statistical properties at different locations along the SWTBLIs investigated

SWTBLI case	Probe location	$\bar{p}_w$(Pa)	σ_p(Pa)	$\sigma_p/\bar{p}_w$	skewness	kurtosis	energy > 10kHz (%)
$\alpha = 3°$	K1	11,271	74	0·007	0·06	3·0	80·7
$\alpha = 9°$	K1	6,793	50	0·007	0·04	3·0	72·9
	K2	12,553	233	0·019	0·16	3·1	79·3
	K3	12,966	295	0·023	0·19	3·0	82·9
$\alpha = 13°$	K1	6,980	198	0·028	1·55	8·5	45·4
	K2	11,740	355	0·030	0·13	3·3	70·2
	K3	15,224	404	0·027	0·16	3·2	73·3
	K4	14,375	411	0·029	0·25	3·2	70·2
	K5	16,338	497	0·030	0·15	3·0	77·5
$\alpha = 15°$	K1	12,508	450	0·036	0·00	3·4	66·7
	K2	13,358	476	0·036	0·01	3·3	65·9
	K3	15,995	474	0·030	0·10	3·0	71·0
	K4	14,890	495	0·033	0·11	3·1	67·6
	K5	17,458	732	0·042	0·21	3·2	71·6

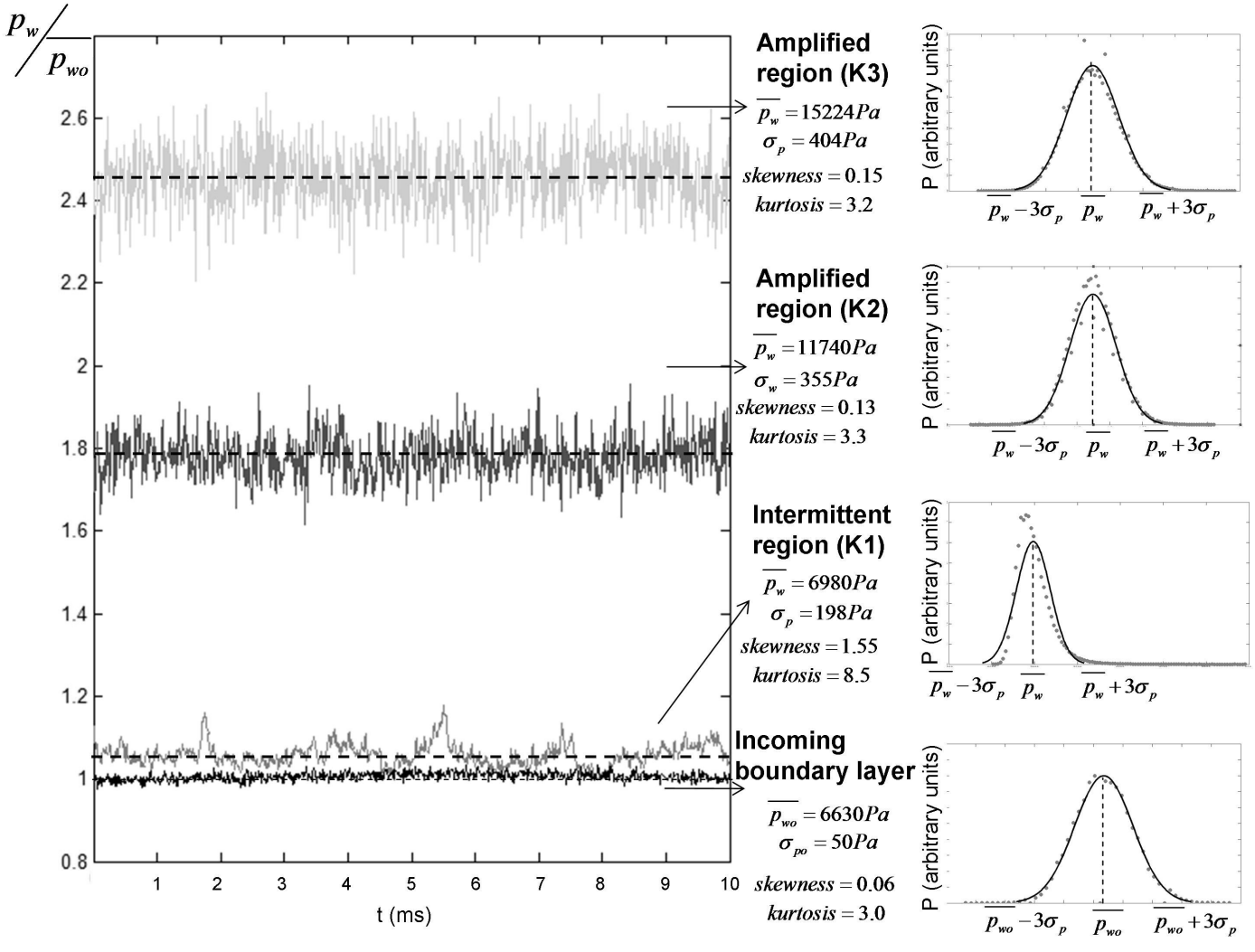
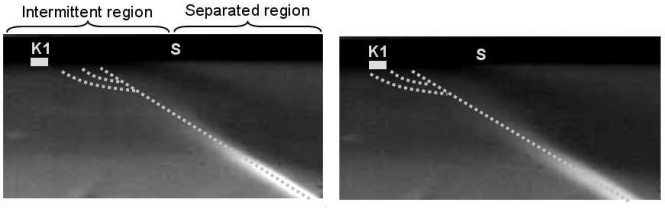


Figure 10. Unsteady pressure signals of undisturbed incoming boundary layer and of K1, K2, K3 signals in $\alpha = 13°$ SWTBLI with corresponding probability distributions.

https://doi.org/10.1017/S0001924000003742 Published online by Cambridge University Press



(a) (b)

Figure 11. Schlieren images indicating mean position of reflected shock $\overline{x_s}$ (a) and maximum upstream displacement of the shock $x_s - \overline{x_s}$ (b) respect K1 location in α = 13° SWTBLI.

critical interactions, pressure starts increasing from the separation region to reach a local maximum at the shock impingement location, to then follow with a slight pressure decrease downstream and subsequently with an even higher increase in pressure as it approaches the reattachment region (see Table 3 and Fig. 5). The shock is thus expected to provoke an amplification of the incoming boundary layer spectral energy. However, despite the apparent linear amplification of the high frequency fluctuations in the undisturbed boundary layer, there appears to be an addition of low-frequency power spectra at some locations in the interaction. This is shown in Fig. 10 for the α = 13° case, which presents the $p_w/\overline{p_{wo}}$ signal at K1, K2 and K3 for a duration of 10ms together with the probability distribution of the total signal and their equivalent Gaussian distributions. The intermittent nature of the flow close to the separation region is reflected in the pressure signal at K1 location. This can also be observed in the high-speed Schlieren results based on the reflected shock's foot location (Fig. 11). Along the rest of the interaction such low frequency intermittency ceases due to the dominant high frequency fluctuations. This trend is similar to that presented by Tran and Bogdonoff[17] on compression corner and fin SWTBLIs.

In the subcritical interaction (α = 3°), whereas there is a local increase in mean pressure and thus in spectral energy, the skewness and kurtosis values are the same as those of the undisturbed boundary layer and most of the energy (≈80%) is still over 10^4Hz. In the critical interaction case (α = 9°), most of the spectral energy at the three measurement locations is also found at frequencies higher than 10^4Hz. The incidence of the shock again appears to produce an amplification of the energy at the shock impingement point as well as at the downstream region. Increased spectral energy in the 10^3Hz-10^4Hz range is found upstream of the interaction which is attributed to its proximity to the incipient separation region. A decrease in spectral energy downstream of the interaction is also observed. The kurtosis value is closely matched to a normal distribution (σ_p = 3) through the interaction. It should also be noted that the standard deviation with respect to the local mean pressure ($\sigma_p/\overline{p_w}$) – also known as the coefficient of variation and provided in Table 3 to offer a non-dimensional measure of the standard deviation – varies slightly along the interactions and increases with the strength of the impinging shock. The variability of the data therefore increases with interaction strength. The skewness factor increases slightly through the interaction, reaching a value of 0·19 downstream of the interaction. A positive skewness value indicates in this case that the distribution is right-skewed, i.e. there are fewer high pressure values and the mean is larger than the median value, while the latter is at the same time larger than the statistical mode. At point K3 and α = 9°, these pressures do not present significant differences: 1,297Pa (mean), 1,296Pa (median) and 1,283Pa (mode).

At α = 13º, (see Fig. 13(a)), a significant low-frequency influence is observed at the K1 transducer location. At this point there is an increase in spectral energy mostly at frequencies in the 10^3Hz-10^4Hz range, where only around 45% of the energy is greater than 10^4Hz in comparison to the 70%-80% along the rest of the interaction. The skewness and kurtosis factors are also significantly different than at the rest of locations, with values of skewness = 1·55 and kurtosis = 8·5. Kurtosis values much higher than 3 indicate that infrequent and

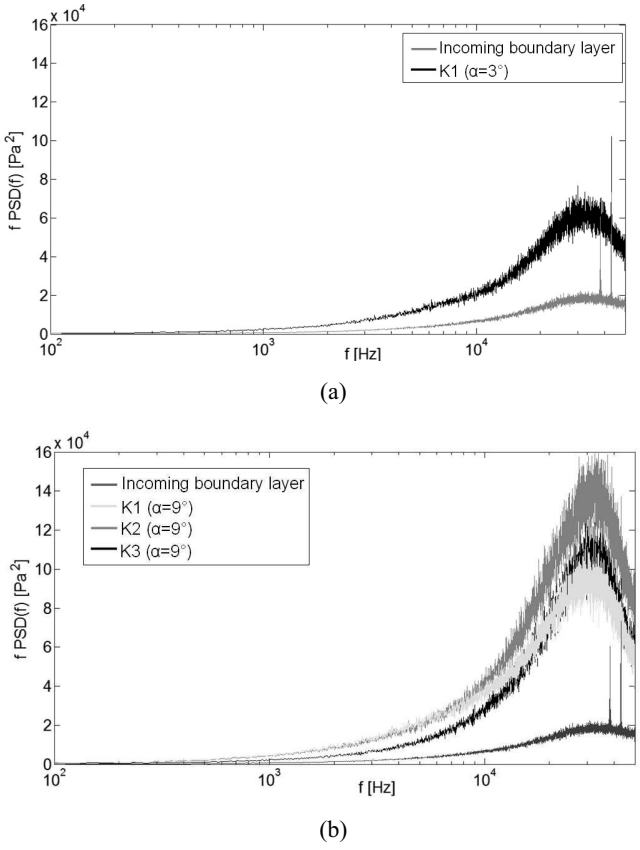


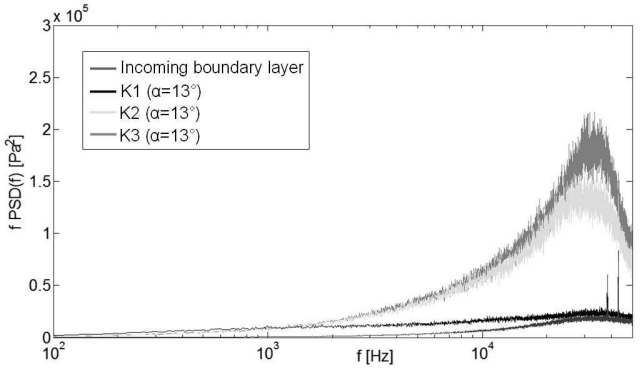
Figure 12. Unsteady pressure measurements corresponding to subcritical interaction α = 3° (a) and to critical interaction α = 9° (b).

severe deviations take place and data is therefore more peaked with heavy tails. This is caused by the stronger low frequency influence in this region, which results in skewness to lower frequency values but with infrequent extreme deviations to higher pressures. In this case, the mean, median and statistical modes are: 6,980Pa, 6,947Pa and 6,928Pa respectively. An intermittency factor was defined by Dolling and Or[32] to represent the fraction of the time during which v p_w is above the maximum pressure of the undisturbed flow as shown in Equation (3). At K1 (α = 13°), γ = 0·89 is measured, which indicates its proximity to the separation locus. Based on the γ-σ_p correlations presented in their work[32] a standard deviation close to zero should be expected at such high γ values, showing good agreement with the present measurements (σ_p = 0·06). Based also on the spectral density plots at this location, the pressure signal clearly appears as a superposition of low-frequency large-amplitude fluctuations on the high-frequency small-amplitude incoming boundary layer signal. A higher increase in mean pressure is observed along the rest of the interaction (K2 – K5, α = 13°) with skewness and kurtosis factors closely matching the characteristics of normal distributions, although slightly skewed to lower pressures and with kurtosis values slightly over 3. Between locations K2 and K3 there is only an increase in frequency fluctuations higher than 10^4Hz and a reduced low frequency fluctuation energy increase is present at the shock impingement location (Fig. 13(a)).

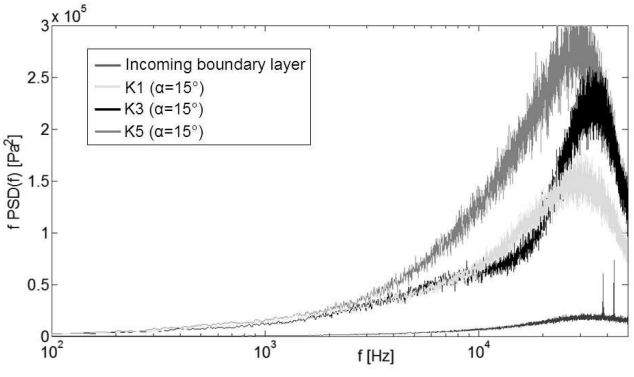
$$\gamma = \frac{time[p > (p_o + 3\sigma_{po})]}{totaltime} \quad \ldots (3)$$

Similar results are observed for the 15º-deflected shock generator case, although measurements could not be taken in the intermittent region of the interaction. Figure 13(b) presents the measurements corresponding to K1, K3 and K5, showing that most of the spectral energy is found in the high-frequency region with a more dominant

https://doi.org/10.1017/S0001924000003742 Published online by Cambridge University Press



(a)



(b)

Figure 13. Unsteady pressure measurements corresponding to two supercritical interactions with α =13° shock generator at K1, K2 and K3 (a) and α = 15° shock generator at K1, K2 and K5 (b). Measurements at the other locations are not plotted for presentation purposes but are listed in Table 3.

low-frequency influence at locations closer to the separating and reattaching flow. There is again a tendency of increasing skewness through the interaction. The kurtosis factors are slightly above 3, except at the shock impingement location (K3) where it is exactly 3·0. The dominant frequency at this location is similar to that of the incoming boundary layer (≈40kHz), indicating that there is a direct amplification. Closer to the separation and reattachment regions the peak in the power spectrum plots is slightly lower and the kurtosis higher, which is thought to be due to a reduction in convection velocity close to these regions as observed by Thomas *et al*[36] in two-dimensional compression ramp SWTBLIs.

A comparison of power spectra plots of the signal under the shock impingement locus for each interaction is presented in Fig. 14. The increased fluctuation energy for larger shock generator deflection angles is observed thus showing the severity of each interaction. It is also observed that for stronger interactions there is a more significant proportion of fluctuation energy at low frequencies (< 10^4 Hz): 19·3% (K1 α = 3°), 20·7% (K2 α = 9°), 26·7% (K3, α = 13°) and 29·0% (K3 α = 15°).

3.4 Summary of results

A summary of the present results is shown in the form of a schematic diagram in Fig. 15. The higher moments (skewness and kurtosis) of the pressure signals obtained in the separated region are practically unaffected with respect to those of the undisturbed boundary layer and an effective amplification of the spectrum is observed. It is at the impingement locus where mostly high

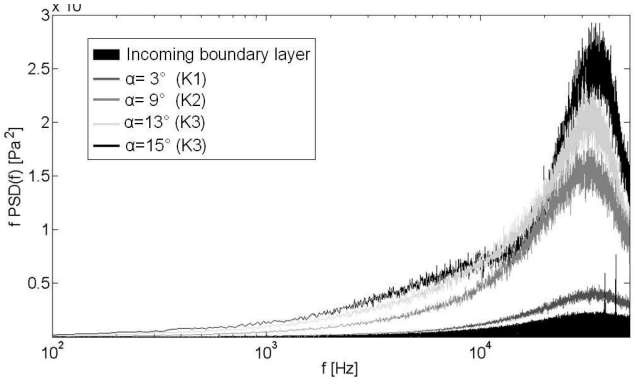


Figure 14. Unsteady pressure measurements under shock impingement location for all interactions investigated and compared with respect to incoming boundary layer.

frequency pressure fluctuations (>10^4Hz) appear to be amplified, while an increased amplification at lower frequencies (>10^3Hz) is noticed close to the separation and reattachment regions.

A markedly different behaviour is observed at separation. The results presented here show an intermittent region characterised by the addition of low frequency energy (<10^4Hz) measured at this location. In addition, based on the free interaction theory[33], these findings are also confirmed through previous similar studies on other types of SWTBLIs, e.g. two-dimensional compression ramps or forward steps[37,38], Fig. 16. Further evidence that also indicates this low-frequency unsteadiness to be related to the separation mechanism of the boundary layer and the associated flow structure is present in the findings of Dolling and Erengil[23], Beresh *et al*[21] and Ganapathisubramani *et al*[24] among others, as reviewed in Section 1.

4.0 CONCLUSIONS

The interaction between an impinging shock wave and a turbulent boundary layer has been studied at a freestream flow Mach number of 2·42. The unsteady behaviour of subcritical, critical and supercritical interactions has been investigated using high-speed Schlieren and high-bandwidth pressure measurements. Different frequency orders have been identified in supercritical SWTBLIs in the 10^2-10^4Hz range. The thickness of the incoming boundary layer has been 5mm and the Reynolds number based on boundary layer thickness 2·6 × 10^4. Subcritical, critical and supercritical interactions have been obtained by using different shock generator configurations.

The incoming boundary layer energy is found to be dominated by high frequencies (>10kHz) and the separation mechanism in supercritical interactions results in the addition of low-frequency unsteadiness. The shock results in an amplification of energy in the high frequency range (≈10^4Hz) at the impingement point. In the region of the main recirculation core of the separation there is only an amplification of high-frequency energy (>10^4Hz). Amplification of lower frequency fluctuations is observed at locations closer to the separation and reattachment points. The results thus suggest the low-frequency unsteadiness of the supercritical interactions is inherent to the separation mechanism of the boundary layer.

ACKNOWLEDGEMENTS

The authors would like to acknowledge Derek Giles for manufacturing the test models and John Thrower for the technical assistance through the experimental programme.

https://doi.org/10.1017/S0001924000003742 Published online by Cambridge University Press

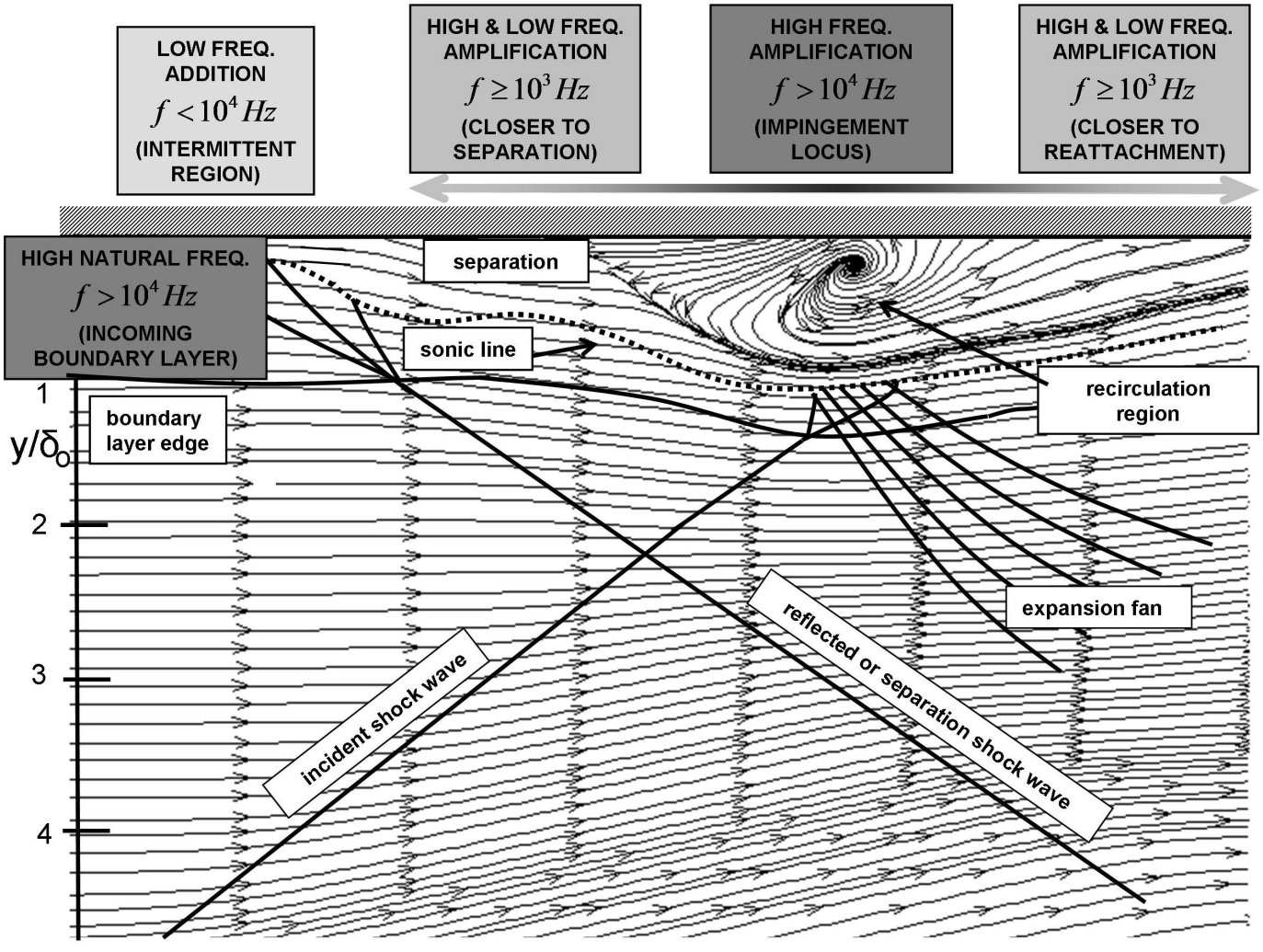
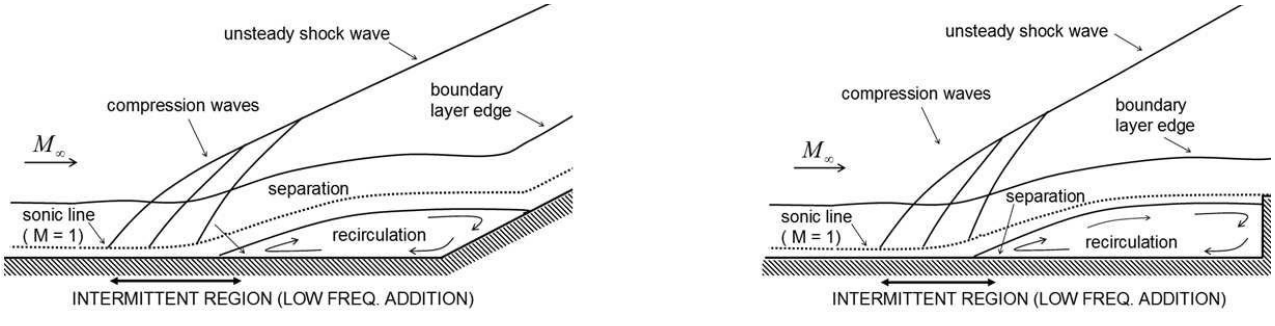


Figure 15. Schematic diagram of present results, flow field based on α = 13° SWTBLI.



(a) (b)

Figure16. Low-frequency influence in other SWTBLIs on 2D compression ramp (a) and forward step (b).

REFERENCES

1. DELERY, J.M. Shock wave/turbulent boundary layer interaction and its control, *Prog Aerospace Sci*, 1985, **22**, (4), pp 209-280.
2. KNIGHT, D. and DEGREZ, G. Shock wave boundary layer interactions in high Mach number flows – a critical survey of current CFD prediction capabilities, AGARD Report 2, 1998, **319**, pp 1-35.
3. DELERY, J. Shock phenomena in high speed aerodynamics: still a source of major concern, *Aeronaut J*, 1999, **103**, (1019), pp 19-34.
4. KNIGHT, D., YAN, H., PANARAS, A. and ZHELTOVODOV, A. RTO WG 10: CFD validation for shock wave turbulent boundary layer interactions, AIAA Paper 2002-0437, 2002.
5. ZHELTOVODOV, A. Some advances in research of shock wave turbulent boundary layer interactions, AIAA Paper 2006-496, 2006.

https://doi.org/10.1017/S0001924000003742 Published online by Cambridge University Press

6. DUSSAUGE, J.P., DUPONT, P. and DEBIEVE, J.F. Unsteadiness in shock wave boundary layer interactions with separation, *Aerospace Sci Technol*, 2006, **10**, (2), pp 85-91.
7. ADAMSON JR., T.C. and MESSITER, A.F. Analysis of two-dimensional interactions between shock waves and boundary layers, *Annual Rev Fluid Mech*, 1980, **12**, pp 103-138.
8. WANG, H.J., YU, S. and CAI, K.J. Unsteadiness of shock wave/boundary layer interaction in supersonic cascade, *Phys Astron*, 1996, **5**, (4), pp 243-247.
9. DELERY, J. and MARVIN, J.G. Turbulent shock wave/boundary-layer interaction, *AGARDograph 280*, February 1986.
10. DOLLING, D.S. Fluctuating loads in shock-wave/turbulent boundary-layer interaction: tutorial and update, 1993, AIAA Paper 93-0284.
11. HEMSCH, M.J. and NIELSEN, J.N. *Tactical Missile Aerodynamics: General Topics*, 1986, AIAA, New York, USA.
12. DOLLING, D.S. Unsteadiness of shock-induced turbulent separated flows – some key questions, 2001, AIAA Paper 2001-2708.
13. DOLLING, D.S. Fifty years of shock-wave/boundary-layer interaction research: what next?, *AIAA J*, 2001, **39**, (8), pp 1517–1531.
14. DUSSAUGE, J.P. and PIPONNIAU, S. Shock/boundary-layer interactions: Possible sources of unsteadiness, *J Fluids Struct*, 2008, **24**, (8), pp 1166-1175.
15. KISTLER, A.L. Fluctuating wall pressure under a separated supersonic flow, *J Acoust Soc*, 1964, **36**, (3), pp 543-550.
16. CHAPMAN, D.R., KUEHN, M.D. and LARSON, K.H. Investigation of separated flows in supersonic and subsonic streams with emphasis on the effect of transition, 1958, NACA Report 1356.
17. TRAN, T.T. and BOGDONOFF, S.M. A study of unsteadiness of shock wave/turbulent boundary layer interactions from fluctuating wall pressure measurements, 1987, AIAA Paper 87-0552.
18. ERENGIL, M.E. and DOLLING, D.S. Correlation of separation shock motion with pressure fluctuations in the incoming boundary layer, *AIAA J*, 1991, **29**, (11), pp 1868-1877.
19. THOMAS, F.O., PUTNAM, C.M. and CHU, H.C. On the mechanism of unsteady shock oscillation in shock wave/turbulent boundary layer interactions, *Exp Fluids*, 1994, **18**, (1-2), pp 69-81.
20. PLOTKIN, K.J. Shock wave oscillation driven by turbulent boundary-layer fluctuations, *AIAA J*, 1975, **13**, (8), pp 1036-1040.
21. BERESH, S.J., CLEMENS, N.T. and DOLLING, D.S. Relationship between upstream turbulent boundary-layer velocity fluctuations and separation shock unsteadiness, *AIAA J*, 2002, **40**, (12), pp 2412-2422.
22. BUENO, P.C., GANAPATHISUBRAMANI, B., CLEMENS, N.T. and DOLLING, D.S. Cinematographic planar imaging of a Mach 2 shock wave/turbulent boundary layer interaction, 2005, AIAA Paper 2005-0441.
23. DOLLING, D.S. and ERENGIL, M.E. Unsteadiness of shock-induced turbulent boundary layer separation – An inherent feature of turbulent flow or solely a wind tunnel phenomenon, August 1994, *Final Rpt Texas Uni*.
24. GANAPATHISUBRAMANI, B., CLEMENS, N.T. and DOLLING, D.S. Effects of upstream boundary layer on the unsteadiness of shock-induced separation, *J Fluid Mech*, 2007, **585**, pp 369-394.
25. DUPONT, P., HADDAD, C., ARDISSONE, J.P. and DEBIEVE, J.F. Space and time organization of a shock wave/turbulent boundary layer interaction, *Aerospace Sci Technol*, 2005, **9**, (7), pp 561-572.
26. ESTRUCH, D., LAWSON, N.J., MACMANUS, D.G., GARRY, K.P. and STOLLERY, J.L. Schlieren visualization of high-speed flows using a continuous LED light source, *J Vis*, 2009, **12**, (4), pp 289-290.
27. ESTRUCH, D., STOLLERY, J.L., MACMANUS, D.G., LAWSON, N.J. and GARRY, K.P. Hypersonic interference heating: a semi-empirical hot spot predictive approach, 2009, AIAA Paper 2009-7444.
28. ESTRUCH, D., LAWSON, N.J. and GARRY, K.P. Application of optical measurement techniques to supersonic and hypersonic aerospace flows, *ASCE J Aero Eng*, 2009, **22**, (4), pp 383-395.
29. ESTRUCH, D., LAWSON, N.J., MACMANUS, D.G., GARRY, K.P. and STOLLERY, J.L. Measurement of shock wave unsteadiness using a high-speed Schlieren system and digital image processing, *Rev Sci Instrum*, 2008, **79**, (12), 126108.
30. OGAWA, H. and BABINSKY, H. Wind-tunnel set up for investigations of normal shock wave/boundary layer interaction control, *AIAA J*, 2006, **44**, (11), pp 2803-2805.
31. KIYA, M. and SASAKI, K. Structure of a turbulent separation bubble, *J Fluid Mech*, 1983, **137**, pp 83–113.
32. DOLLING, D.S. and OR, C.T. Unsteadiness of the shock wave structure in attached and separated compression ramp flows, *Exp Fluids*, 1985, **3**, (1), pp 24-32.
33. BIES, D.A. A review of flight and wind tunnel measurements of boundary layer pressure fluctuations and induced structural response, NASA CR-626, 1966.
34. LAGANELLI, A.L., MARTELLUCI, A. and SHAW, L.L. Wall pressure fluctuations in attached boundary layer flow, *AIAA J*, 1983, **21**, pp 495-502.
35. KUEHN, D.M. Experimental investigation of the pressure rise required for the incipient separation of the turbulent boundary layers in two-dimensional supersonic flow, 1959, NASA Mem 1-21-59A.
36. THOMAS, F.O., PUTNAM, C.M. and CHU, H.C. Measurement of the nonlinear spectral dynamics characterizing a shock wave/turbulent boundary layer interaction, 1991, AIAA Paper 91-0653.
37. MUCK, K.C., DUSSAUGE, J.P. and BOGDONOFF, S.M. Structure of the wall pressure fluctuations in a shock-induced separated turbulent flow, 1985, AIAA Paper 85-0179.
38. ANDREOPOULOS, J. and MUCK, K.C. Some new aspects of the shock-wave/boundary-layer interaction in compression-ramp flows, *J Fluid Mech*, 1987, **180**, pp 405-428.

https://doi.org/10.1017/S0001924000003742 Published online by Cambridge University Press